Journal of
Materials Chemistry B

Materials for biology and medicine

Accepted Manuscript

This article can be cited before page numbers have been issued, to do this please use: P. K. Pandey, P. Chand, K. Rawat, T. Prasad and H. B. B. Bohidar, *J. Mater. Chem. B*, 2020, DOI: 10.1039/C9TB01863H.

ROYAL SOCIETY OF CHEMISTRY

rsc.li/materials-b

Multifunctional, fluorescent DNA derived carbon dots for biomedical applications: bioimaging, luminescent DNA hydrogels and dopamine detection

Pankaj Kumar Pandey[1], Preeti[2], Kamla Rawat[3], Tulika Prasad[2,4]* and H. B. Bohidar[1,2]*

[1]School of Physical Sciences, Jawaharlal Nehru University, New Delhi, India

[2]Special Centre for Nanoscience, Jawaharlal Nehru University, New Delhi, India

[3]Department of Chemistry, School of Chemical and Life Science, Jamia Hamdard, New Delhi, India

[4]Advanced Instrumentation Research and Facility, Jawaharlal Nehru University, New Delhi, India

Abstract

Here, we describe synthesis of 2-3 nm, hydrophilic, blue fluorescence emitting carbon dots (C-Dots, made using DNA precursor) by hydrothermal route from the gelling concentration of 2% (w/v) DNA. These dots exhibited highly efficient internalization in pathogenic fungal cells, negligible cytotoxicity, good PL stability and high biocompatibility, demonstrating their potential as nanotrackers for microbial studies. Bioimaging was performed using *Candida albicans* as representative for microbial pathogens. The novelty of these dots are that they formed fluorescent nanocomposite hydrogel with the same DNA, much below gelation concentration (1 % w/v) and possessed tunable gels of strength between 20 and 80 Pa with corresponding gelation temperature T_{gel} between 40 to 50°C. The network density and gelation free energy data supported superior crosslinking ability of these dots. The as prepared hydrogels can replace existing toxic quantum dots based hydrogels for drug delivery. We also demonstrated the use of DNA hydrogel fabricated working electrode (DNA-C-Dot/ITO electrode) for biosensing of dopamine. Our electrochemical biosensor had a detection limit of 5×10^{-3} mM for dopamine. These multifunctional, fluorescent C-Dots and hydrogel, after suitable conjugation or loading with molecules and drugs hold promising potential for further exploitation in bioimaging, targeted drug delivery, wound healing and biosensing applications.

View Article Online
DOI: 10.1039/C9TB01863H

Introduction

Biotemplated nanostructures offer advantages of high solubility, low toxicity and high biodegradability. Deoxyribonucleic acid (DNA) in recent times has emerged as favoured material for nanostructures with applications in biomedicine and biotechnology. DNA is central genetic molecule of biosystems and is a biopolymer of nucleotides (cytosine, guanine, adenine and thymine) deoxyribose sugar and phosphate. The self-recognition properties of DNA serves as a building block for designing several DNA nanostructures.[1,2,3] Such nanostructures are biocompatible with wide range of applications in material science, analytical science and biomedicine (diagnostics, bioimaging, biosensing and drug delivery) and they can be modulated at nanometer spatial resolution with unique structures and functions.[1]

An unmet need exists for trackable, bioimaging probes with tunable properties, biocompatibility, high photostability and quantum yield. Traditional dyes and fluorophores, presently used for bioimaging have drawbacks of multiple synthetic steps, high cost of production, rapid photobleaching, small Stokes shift, short fluorescence lifetime, narrow excitation spectra and broad emission band.[4,5] Latest developments in nanotechnology have generated high value optical probes to overcome the limitations of fluorophores and traditional dyes.[6] Conventional semiconductor quantum dots (QDs), in the recent years, have found applications in solar cells, photodetectors, cell bioimaging and fluorescent hydrogels.[7–10] These QDs have shown several advantages over traditional fluorescent probes such as broad excitation and narrow emission spectra, long luminescence lifetime, negligible photobleaching and high quantum yield but their toxicity limits their biological use. [7–10] Carbon-based quantum dots (CDs) have emerged as alternative luminescent nanomaterials because of their low toxicity, high photoluminescence, high biocompatibility and low photobleaching properties.[11-14] Absence of heavy metals in CDs unlike the QDs bypasses the environmental hazards and health concerns.[4] However, nucleic acid based dots exhibited photoluminescence with lifetime (~10.44 ns) much longer than carbon dots (< 0.5 ns), making them excellent contender for biomedical and bioimaging (*in vitro* and *in vivo*) uses.[15,16] Fluorescent DNA based nanostructures are therefore, well suited for biological applications. Engineering DNA based nanostructures would certainly provide an imaging modality for tracking in live systems without interference in normal biological functions.

Crosslinking of DNA chains to form semiflexible porous hydrogel is well documented for pharmaceutical applications as drugs carriers, tissue engineering, cell transplantation etc.[17] The DNA hydrogels endow large surface area, high drug loading capacity, tunable mechanical

View Article Online
DOI: 10.1039/C9TB01863H

viscoelastic properties, high stability, triggered biodegradation behavior and enhanced ability for biological interactions, thereby providing promising scope in controlled and targeted drug delivery.[7,18-20] Use of QD- DNA hydrogels for delivery of anti-cancer drug, doxorubicin was reported to increase 9-fold potency against cancer cells.[7] Such DNA based hydrogels would be more versatile for drug delivery and therapy applications as compared to existing toxic quantum dot based hydrogels.[18]

The ability to construct electrochemical sensor based on DNA nanostructures can be beneficial in developing inexpensive multiplexed electrochemical platforms. Although various detection procedures are present for the detection of neurotransmitters *in vivo*, only limited detection methods able to probe analyte selective response with sub-second temporal resolution. The catecholamine dopamine is a widely studied neurotransmitter with multifaceted importance in neurobiological systems and has essential role in neurological pathways. This biological significance makes dopamine an ideal choice for developing a platform for its electrochemical detection. Several electrochemical sensor for dopamine have been reported such as polymer based hybrid materials like $CuInS_2$ QDs, organic electrochemical transistor made with different gate electrodes (multi-walled carbon nanotube-Chitosan hybrid, Graphite, Au and Pt based electrode) and recent PEDOT:PSS based sensor.[21-24] But there remains a need for dopamine sensor with high specificity and sensitivity, fast response time and low detection limit.

In this study, we synthesized carbon dots (C-Dots) from ds-DNA and investigated their multifunctional potential. We demonstrated the application of these C-Dots for bioimaging using the fungal (eukaryotic) pathogen, *Candida albicans*. This opportunistic pathogen was used as a representative for microbial pathogens. Further these dots efficiently internalized into the fungal cells and exhibited negligible toxicity. Interestingly, we for the first time show the synthesis of fluorescent DNA hydrogel at low concentration with the C-Dots working as crosslinker. The dots were also optimized for selective detection of dopamine using the electrochemical platform. Because of the advantages, multifunctional systems based on DNA nanostructures can be designed to develop biomedical applications such as drug delivery, clinical therapy, bioimaging and biosensing. Functional DNAs with desired modifications hold ability for versatility in nanotechnology and bioanalysis and appear as a promising material for assembling DNA nano-architectures for use in biomedicine and nano-biotechnology.

View Article Online
DOI: 10.1039/C9TB01863H

Material and Methods

Materials

Salmon testes DNA (2000 bp, ds DNA, nominal MW= 2 KDa) was purchased from Sigma-Aldrich (USA). For culturing microbial cells, the media chemicals (i.e. Yeast extract, Peptone, Glucose and Agar) were obtained from Fisher Scientific (Mumbai, India) and HI-Media (Mumbai, India). Analytical grade NaCl, KCl, Na_2HPO_4 and KH_2PO_4 for preparing buffers and hydrogen peroxide solution were also obtained from Fisher Scientific (Mumbai, India). All solvents such as water, Methanol and Ethanol were of high purity HPLC grade and procured from Merck. Fluorescent probe 2, 7, Dichlorofluorescin Diacetate (DCFH-DA), L-cysteine (L-Cys), dopamine (Dop) and Glycine (Gly) was procured from Sigma Chemical Co. (St. Louis, Mo. USA). ITO (indium-tin oxide, Sn:In2O3) glass sheets were purchased from Balzers, UK (1.1 mm thick, 90 % transparent and 25 Ω sq^{-1} surface plate resistance). $K_4Fe(CN)_6$ and $K_3Fe(CN)_6$ were purchased from SRL, India. All procedures were performed at room temperature of 25^0 C unless stated otherwise.

UV-Visible spectroscopy

UV-Vis absorbance spectra were recorded using Agilent, Carry 60 UV-Vis spectrophotometer (USA) with help of two sided optically clear quartz cell of 10 mm path length.

Fluorescence spectroscopy

Fluorescence emission spectra of samples were recorded with help of (Carry Eclipse, Agilent, USA) Fluorescence Spectrometer using four side optically clear quartz cell of 10 mm of path length.

Transmission Electron Microscopy

Particle size histogram was obtained using transmission electron microscope (TEM), JEOL 2100 (USA) operating at 200 kV and 1,000,000X magnification. The sonicated sample was drop casted onto the carbon coated Cu-grid for imaging.

View Article Online
DOI: 10.1039/C9TB01863H

X-Ray Diffraction

X-ray Diffraction (XRD) spectrum of sample was recorded with the help of PANalytical X'pert PRO system.

Zeta Potential

Zeta-potential of the samples were measured by ZEECOM instrument (Model: No.ZC-2000, Microtec, Japan), taking into account the immediate estimation of electrophoretic mobility under voltage settled at 30 V.[25]

Dynamic Light Scattering

Dynamic Light scattering instrument (DLS) (PhotoCOR instruments, USA) mounted on a vibration isolation table and activated in multi-tau mode was used for determining particle size. The particle size histogram was determined from Laplace inversion of measured intensity correlation function $g_2(\tau)$. More discussion about DLS can be found in ref.[26]

Atomic Force Microscopy

The surface map was imaged by atomic force microscopy (AFM) using WITec Instrument GmbH, Germany.

Rheology Measurement

To probe viscoelastic properties, rheological measurements were performed on an AR 500 Rheometer, (TA instrument, England) using the (2^0) cone plate geometry.[20]

Field Emission Scanning Electron Microscope

Surface morphology of the freeze dried hydrogel was assessed by Field Emission Scanning Electron Microscopy (FESEM) using Tescan, LYRA 3 XMU, Czech Republic. The imaging was performed on gold coated hydrogel sample.

Fourier-transform infrared spectroscopy

FTIR spectra were taken on a Varian FTS7000 FTIR spectrometer. The instrument used 10 mm path length cuvettes for liquid samples.

Energy Dispersive X-Ray Microanalysis

View Article Online
DOI: 10.1039/D0TB01863H

EDX (Energy Dispersive X-Ray Microanalysis) was done by Scanning Electron Microscope (SEM) - Zeiss EVO40.

Synthesis of DNA based Carbon Dots (C-Dots)

The easiest method for DNA based carbon dots (C-Dots) synthesis was a single step process using gelling concentration of salmon DNA (2% (w/v)) as precursor. It was heated to 60°C with continuous stirring on magnetic stirrer for 1 h. After one hour, the resulting homogeneous solution was transferred to Teflon coated autoclave and kept overnight in heating oven at 200°C. The obtained material was allowed to cool to room temperature (25°C) and purified by centrifugation at 1000 rpm followed by dialysis performed overnight against deionized water using a membrane of MWCO= 10 kD.

Growth media and Microbial strain used

Candida albicans SC5314 was used as pathogenic fungal test organism and description of strain is already described before.[27] The microbial strain was cultured at 30°C in broth containing 2% (w/v) Dextrose, 2% (w/v) Peptone and 1% (w/v) Yeast extract. For solid YEPD plates, 2.5% (w/v) Agar was added to broth. The cells were grown for 14-16 hours with shaking at 140-150 rpm at 30°C. All experiments were conducted in triplicates using exponential phase fungal cells and average of three independent experiments along with standard deviation was calculated. GraphPad Prism version 5.0 (GraphPad software, CA) was used to calculate *p*-value in Student *t*-test for validating reproducibility and significance of experiments, wherein significance was indicated by p value < 0.05.

Microbial toxicity of C-Dots

The toxicity of C-Dots was assessed using broth microdilution dilution assay in accordance to recommendations of Clinical and Laboratory Standard Institute (CLSI).[28,29] Mid-exponential log phase cells grown on solid agar plates were resuspended to an optical density of 0.1at 600 nm i.e. (OD_{600}) in 0.9 % saline, (corresponding to cell number 0.5 – 1 x10^6 cells/ml). Subsequently, final concentration of cells is made upto 0.5 – 1 x 10^4 cells/ml by further 100-fold dilution in YEPD medium. These cells were grown at 30°C in presence of different concentrations of C-Dots. The growth of cells was evaluated by taking OD_{600nm} in

View Article Online
DOI: 10.1039/C9TB01863H

microtitre plate reader and also confirmed visually. Growth control was maintained without C-Dots.

Intracellular Reactive Oxygen Species (ROS)

Assessment of intracellular ROS in fungal cells was carried out using a fluorogenic cell permeant dye, DCFH-DA as described before.[30] Mid-exponential phase cells grown in absence of C-Dots (control), presence of C-Dots (4 and 8 mg/ml) and 10 mM H_2O_2 (positive control) were harvested by centrifugation at 5000 rpm for 10 mins at 4ºC and washed thoroughly with PBS buffer (pH 7.4) to remove media. Finally, 10^7 cells were re-suspended in 3 ml PBS (pH 8.4). Then, DCFH-DA was added to final concentration of 10 µM to each cell suspension followed by incubation for 1 hr at 30°C. Relative fluorescence (Rf) Intensity was acquired at 488 nm excitation and 540 nm emission wavelengths in a Perkin Elmer L55 spectrofluorimeter using respective slit widths of 5 and 10 nm. The effect of auto-fluorescence was eliminated separately by using blank (no fluorescent probe). The fluorescent cells were imaged using the confocal microscope *FluoView™ FV1000* and the fluorescence inside the cells indicated intracellular ROS**.**

Cellular uptake of C-Dots by fungal cells

The uptake of C-Dots by fungal cells was quantitated to assess their internalization following the method described earlier with slight modifications.[31] Mid-exponential phase grown fungal cells were harvested and washed with thoroughly with PBS buffer (pH 7.4). The washed cells were then resuspended in PBS (pH 7.4) to a concentration of 10^7 cells/ml and incubated with C-Dots to final concentration of 4 mg/ml. From this cell suspension, aliquots of 10^7 cells were taken out at following time points viz. 30 min, 1, 2, 4, 8 and 14 hrs. The cells taken out at each time point were harvested to remove supernatant followed by resuspension in 1 ml PBS. The relative fluorescence Intensity (*Rf*) was measured at excitation and emission wavelengths of 350 and 450 nm respectively using Perkin Elmer L55 spectrofluorimeter with slit widths of 10 nm. Separate blank (no C-Dots) was maintained to eliminate effect of auto-fluorescence. Rhodamine 6G (R6G), a highly fluorescent tracer dye at concentration of 10 µM was used as positive control. The cellular uptake for R6G was measured using spectrofluorimeter at 488 nm excitation and 530 nm emission wavelengths with 10 nm slit widths.

View Article Online
DOI: 10.1039/C9TB01863H

Fluorescence Microscopy

The presence of C-Dots within the cells was visually detected by fluorescence inside the cells using the Zeiss Imager Z1 apotome microscope. The fungal cells were incubated with C-Dots separately at respective concentrations of 4 mg/ml and 8 mg/ml for 30 mins, 1 hr and 2 hrs, subsequent to which cells were thoroughly washed and resuspended in PBS. Images were recorded with the help of cooled monochrome CDD camera AxioCam HRm with Axiovision Rel 4.8.1 software. Rhodamine 6G at the concentration of 10μM was used as positive control to check cellular uptake of the dye.

Synthesis of Fluorescent DNA-C-Dot hydrogel

2 % (w/v) DNA was dissolved in deionized water and heated to 60°C with stirring for 60 min, which resulted in a homogeneous and optically clear solution. Previously synthesized carbon dot sample (0.8 to 4 % (w/v)) was then added to hot DNA solution such that final concentration of DNA was 1 % (w/v) in the DNA-C-Dot sol. These samples were allowed to cool to room temperature to attain gelation (DNA –C-Dot hydrogel), which was established from the non-flowing meniscus of nascent gel held inside a test tube, when inverted.

Electrochemical sensing

Electrochemical sensing of analytes was performed via Cyclic voltammetry (CV) studies on a Autolab Potentiostat/ Galvanostat (Eco Chemie, Netherlands) using a three anode cell in connected potential range of - 0.05 to 0.5 V. The three electrodes used were working electrode (DNA-C-Dot/ITO), auxiliary electrode (Pt-wire) and reference electrode (Ag/AgCl). The CV studies were conducted using Zobell's solution (3.3 mM$K_4Fe(CN)_6$, 3.3 mM $K_3Fe(CN)_6$ with 0.1 M KCl at pH 7). Analyte concentration was standardized by repeating the experiments thrice under similar experimental conditions.

The different analytes used in the study were Urea (U), Citric acid (CA), L-cysteine (L-Cys), dopamine (Dop), and Glycine (Gly). 100 mM stock solution of these analytes were prepared separately in deionized water and stored at 4°C when not in use.

Results and Discussion

Characterization of C-Dots

As synthesized water soluble DD's were characterized by TEM and a typical image is shown in Fig. 1(A). The average size of C-Dot was estimated using ImageJ software. The size histogram (Fig. 1(C)) showed that average size for C-Dot was 3 nm and interplanar spacing was 0.15 nm (Fig. 1(B)). More TEM images are given in Fig. S2 (Supplementary Information). Intensity auto-correlation function was measured by DLS and corresponding size distribution histogram is given in Fig. S3 (Supplementary Information) which yields a mean particle size of ~ 4-5 nm. The AFM images (Fig. 1(F)) from the height profile analysis yield a mean size of ~ 6 nm. Thus, the TEM, AFM and DLS techniques provided coherent information on particle size.

X-ray diffraction pattern of synthesized C-Dots in Fig. 1(D) shows intense diffraction peaks at 260 which corresponds to (002) crystalline plane. Scherrer formula[32] gave estimation about average crystallite size (6 nm). The uniform C-Dot film was prepared using a spin coater. The spin coating of the sol on the ITO/glass substrate was done by gradual spinning at 500 rpm for 10 s, followed by 4000 rpm for 30 s. Then, the film was dried in a vacuum desiccator for 24 hr. the dispersion of DD on a mica substrate followed by drying. The AFM image in Fig. 1(F) revealed the height profiles with the mean size of 3 ± 3 nm. UV- visible spectra shown in Fig. 1(E) clearly shows signature absorption peak for DNA at 260 nm, and for DD at 260 and 360 nm. The optical band gap was determined by using Tauc's equation[33] given by,

$$(\boldsymbol{\alpha h\upsilon})^2 = \boldsymbol{\beta}(\boldsymbol{h\upsilon} - \boldsymbol{E_g}) \qquad (1)$$

where α is absorption coefficient, absorption coefficient is given by α, β is band tailing parameter, ν is photon frequency, h is Planck's constant and E_g is required optical band gap. The band gap from linear fitting of plot $(\alpha h\nu)^2$ vs hν yielded a value of 3.80 eV (Fig. S1, Supplementary Information). When the sample was UV excited at 360 nm, a clear 450 nm blue fluorescence light was emitted which is depicted in Fig. 1(E). The surface charge on the C-Dots was confirmed from the zeta potential histogram shown in the Fig. 1(G), which ascribes a mean zeta potential of -6.5 mV to these particles.

View Article Online
DOI: 10.1039/C9TB01863H

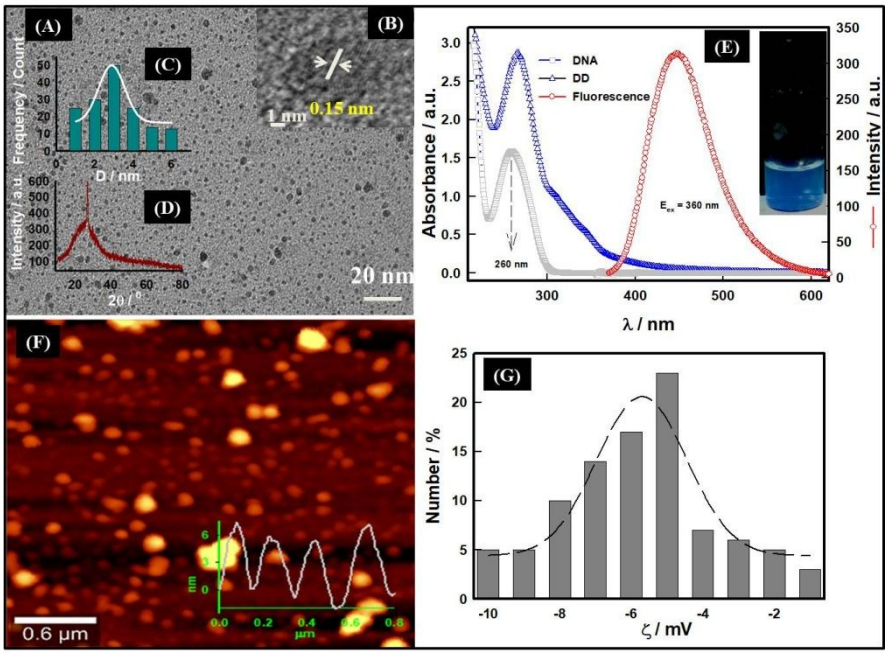

Fig. 1. Characterization of C-Dots: (A) TEM image, (B) Interplanar spacing, (C) Size histogram obtained from TEM image analysis using imageJ software, (D) XRD pattern, (E) UV-fluorescence spectra (inset shows sample under UV-light), (F) AFM image (inset shows height distribution) and (G) Zeta potential histogram.

The chemical composition of the dots was identified by EDX. In order to determine the elemental composition, the weight and atomic ratios of C, N, P and O of the sample were obtained from the EDX data (Fig. 2(A)), which clearly shows the propensity of carbon in these samples.

The FTIR spectra shows (Fig. 2(B)) a sharp absorption peak at 3014 cm^{-1}, which resulted from the stretching of N-H group. The characteristic absorption peak located at 3458 cm^{-1} arose from the -NH stretching, and the 3726 cm^{-1} peak was due to the –NH bond. The 1739 cm^{-1} peak came from the C = O band stretching. C = O and -N-H bonds were involved in the hydrogen bonding with in the secondary structure of DNA. Peak at 1739 cm^{-1} was corresponding to C = O stretching vibration, 1215 cm^{-1} and 1366 cm^{-1} were due to C-H bending vibrations. Sharp peak seen at 1094 cm^{-1} is due to phosphate symmetric vibration. This peak is clearly seen in the C-Dot spectra implying it owed its origin to the DNA precursor.

Excitation dependent emission data is shown in (Fig. 2(C)) which is a clear signature of dot formation. It was clear that the emission intensity was dependent on the excitation wavelength

View Article Online
DOI: 10.1039/C9TB01863H

λ_{ex} (Fig. 2(D)). The fluorescence spectra of the dots varied systematically with the excitation wavelength in the probed region of λ_{ex} = 290–380 nm. A strong emission peak located at λ_{em} =450 nm was observed when the excitation wavelength was λ_{ex} = 350 nm. The emission peak was also shifted to a higher wavelength with the increase of the excitation wavelength, which is indicative of the mechanism of fluorescence behavior of these dots. The main causes for this behavior may be attributed to the presence of dots of different size, and the heterogeneous distribution of surface energy traps on these C-Dots.

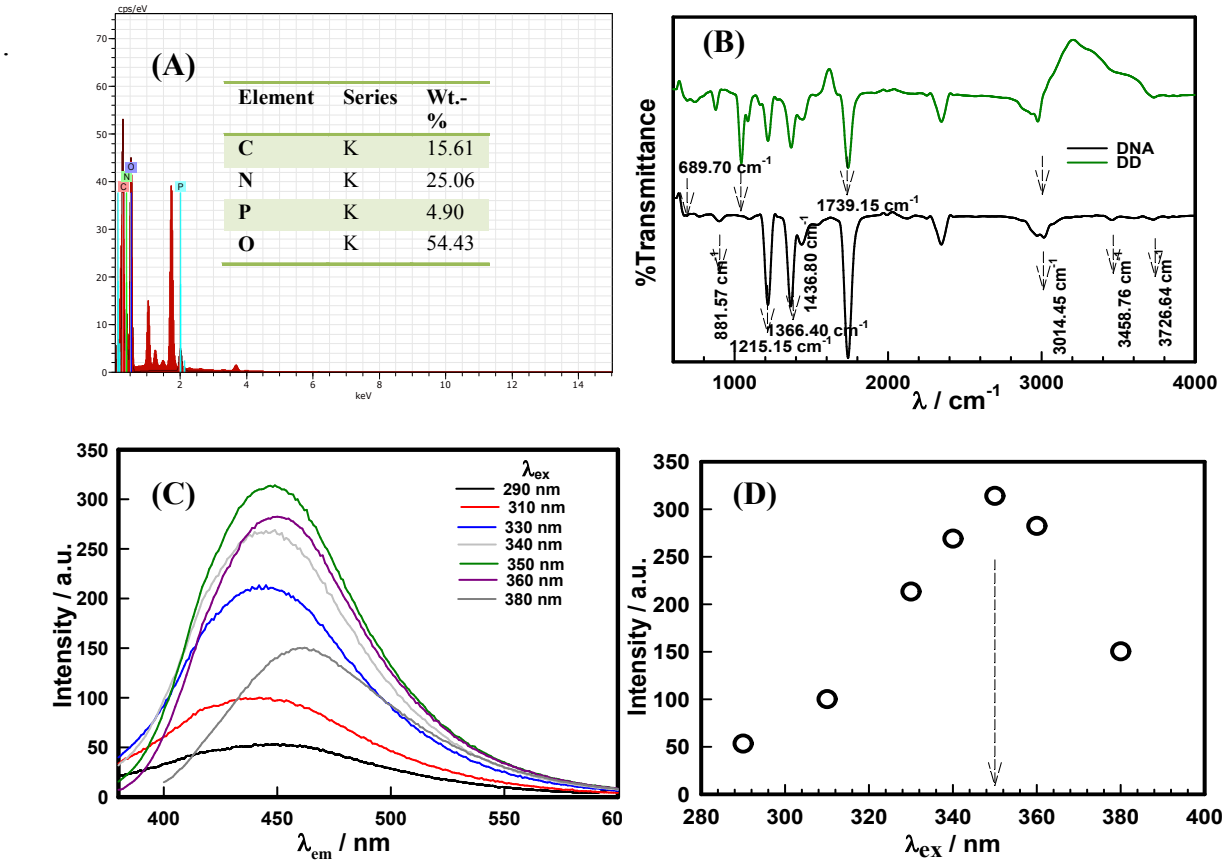

Fig. 2. Characterization of C-Dots: (A) EDX image (Inset table shows the elemental composition), (B) FTIR spectra, (C) Excitation dependent emission data, and (D) emission intensity at 350 nm for various excitation.

Microbial toxicity of C-Dots

C-Dots are a new class of fluorescent nanodots derived from DNA and are nanomaterials with photoluminescence, biocompatible, low-cost and environment friendly

View Article Online
DOI: 10.1039/C9TB01863H

properties.[34] C-Dots are more biocompatible than other nanomaterials since their backbone is constituted by the non-toxic elements.[35] C-Dots being non biotoxic, fulfill the basic requisite for bio-applications such as imaging. Many research groups have evaluated the toxicity of C-Dots against various cancer cell lines and reported that cells could withstand a very high dose of C-Dots for very long duration of time without any change in cell viability.

The application of the C-Dots in bioimaging was demonstrated using microbial pathogen, *Candida albicans*. For this, microbial toxicity of C-Dots was first determined using broth microdilution method. Results of broth micro-dilution assay revealed that there was no change in optical density of the cells even after 48 hours of incubation of cells with very high concentration of 8 mg/ml C-Dots, implying that viability of fungal cells remained unaffected by C-Dots (Fig. 3(A)). The effect of C-Dots on growth of fungal cells was determined by comparing percentage of growth of fungal cells in presence of C-Dots with that of control (absence of C-Dots). We found that there was no inhibition in growth even after incubating the cells for 48 hours up to a high concentration of 8 mg/ml (Fig. 3(B)).

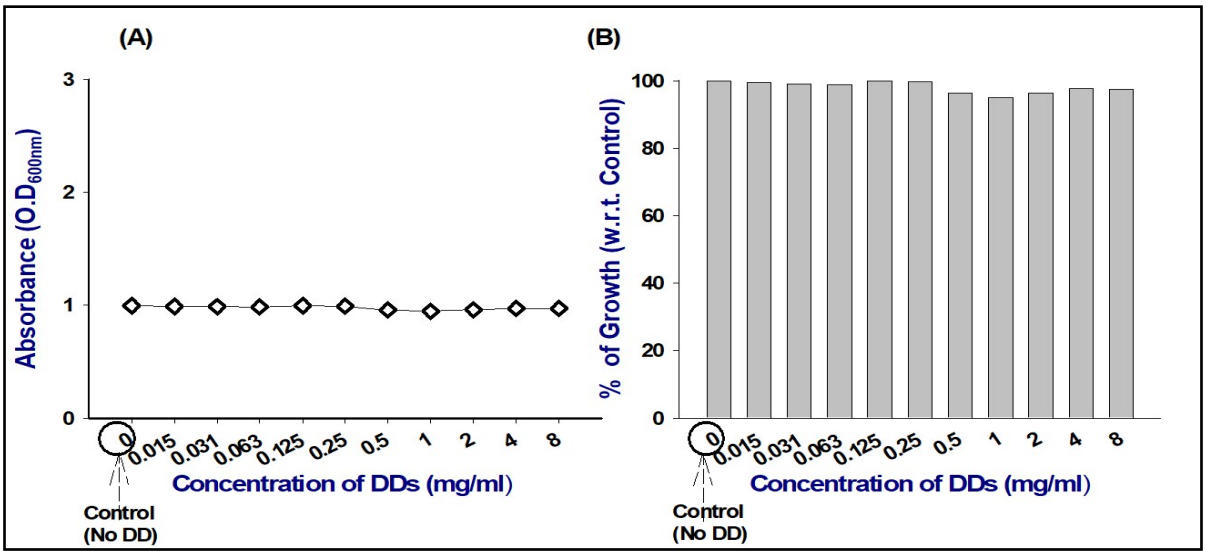

Fig. 3. Microbial toxicity of C-Dots (DDs) towards fungal cells determined by broth microdilution method. (A) Determination of absorbance (OD_{600nm}) of fungal cells grown in absence (Control) and presence of C-Dots respectively. The values on Y axis indicate the optical density of fungal cells represented as means ± SD of three independent experimental sets. (B) Percentage of growth of fungal cells grown in the presence of various concentrations of C-Dots and calculated with respect to Control (absence of C-Dots). The values represent means ± SD of three independent experimental sets.

View Article Online
DOI: 10.1039/C9TB01863H

Intracellular ROS induced by C-Dots

Nanomaterials are known to induce cytotoxicity through augmentation of intracellular ROS, which is known to exert cytotoxic effect through induction of mitochondrial dysfunctional apoptosis by hydroxyl radicals.[36]

Endogenous ROS generated due to C-Dots in fungal cells was measured in this study using the cell permeant fluorogenic dye, DCFH-DA. After diffusion into the cells, cellular esterases deacetylate the dye to form stable and colorless dichlorofluorescein, which is further oxidized by intracellular ROS to produce fluorescent, 2,7- dichlorofluorescein (DCF). It is well understood that higher amount of intracellular ROS will lead to higher intracellular fluorescence due to increased production of DCF.[30] However, it was found that as compared to the basal intracellular ROS levels in control (no C-Dots), there was no change in intracellular ROS levels of cells incubated with 4 and 8 mg/ml C-Dots respectively (Fig. 4). The data obtained through fluorescence measurements for generation of intracellular ROS was well in agreement with results of confocal microscopy (Fig. 4), wherein comparable fluorescence intensity was observed within control (no C-Dots) and fungal cells incubated with C-Dots, thus implying similar levels of intracellular ROS (Fig. 4). The H_2O_2 treated cells were used as positive control (Fig. 4a and 3b).

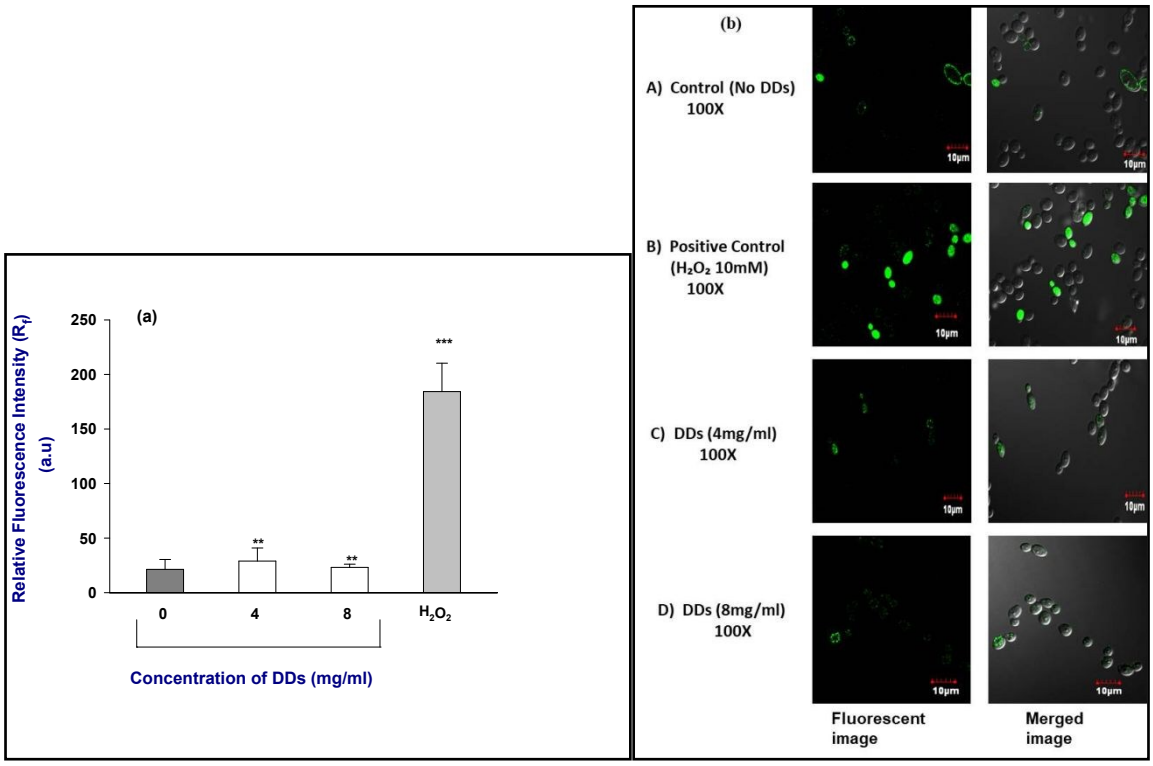

Fig. 4. Estimation of Intracellular ROS production. (a) Quantitation of intracellular ROS in the fungal cells grown in absence and presence of C-Dots (DDs) (4 and 8 mg/ml) using DCFH-

DA fluorescent dye; ROS levels are measured as relative fluorescence (Rf) intensity and Y axis depict the mean Rf values ± the standard deviation (SD) of three independent experimental sets; Rf intensity for cells incubated without DCFH-DA (blank) was subtracted from Rf intensity for cells incubated with DCFH-DA to calculate final Rf intensity.[29] ** represents $p<0.001$ and *** represents $p<0.0001$ calculated with respect to "no C-Dots" (control), (b) Confocal images showing intracellular ROS as green fluorescence within the fungal cells grown in the absence (panel A) and presence of 4 mg/ml and 8 mg/ml C-Dots (panels B and C), respectively. The left panels depict the fluorescence images (higher fluorescence implies higher ROS production) and each right panel shows the merge for the phase-contrast micrographs and fluorescence images at 100X magnification. The results for cells treated with C-Dots were compared to the control cells (no C-Dots; panel D) and positive control (cells treated with 10 mM H_2O_2 (hydrogen peroxide); panel D).

It is envisioned in this study that the C-Dots were nontoxic towards the microbial cells tested, mainly because they were not able to augment generation of intracellular ROS unlike other nanomaterials. The above data suggests a promising future potential of our non-toxic C-Dots for further biomedical and bioimaging applications.

Cellular uptake

For evaluating the potential of C-Dots in bioimaging, the primary prerequisites remain their non cytotoxicity and internalization into the cells. The internalization of C-Dots within microbial cells is determined by their cellular uptake.[37] As a new family of nanomaterials, C-Dots have been reported to penetrate the plasma membrane due to their small size and show fluorescence inside the cells. Cellular uptake of C-Dots is reported to be time, dose and partially energy dependent through passive diffusion.[38] Red-emitting C-Dots have been reported to exhibit incubation time dependent cytoplasmic accumulation in HeLa cells, thus confirming their uptake by passive diffusion.[34]

For predicting the use of C-Dots for bioimaging in microbial cells and other biomedical applications, the cellular uptake of C-Dots was quantified using spectrofluorometer in terms of fluorescence intensity after incubation with 4 mg/ml C-Dots for 30 mins, 1 hr, 2 hrs, 4 hrs, 8 hrs and 14 hrs. Time dependent kinetics for cellular uptake revealed highest intracellular concentration of C-Dots after 30 mins incubation (Fig. 5) which is evident from the high fluorescence intensity due to presence of C-Dots in fungal cells. It appears that the C-Dots enter

View Article Online
DOI: 10.1039/C9TB01863H

the cells by passive diffusion and accumulate in the cytoplasm to attain saturation, reaching the highest intracellular concentration at 30 mins (Fig. 5). Gradually equilibrium was attained to maintain intracellular levels of C-Dots till 14 hrs (Fig. 5). R6G is well known fluorescent tracer dye used for real-time monitoring of cellular processes such as sub-cellular localization, biological functionality, membrane transport processes, diffusion and kinetics.[39] R6G is known to enter *Candida cells* by passive diffusion and was used as a positive control in this study.[29,30] The cellular uptake of 10 µM R6G was monitored after incubation for the same time periods of 30 mins, 1 hr, 2 hrs, 4 hrs, 8 hrs and 14 hrs and it was found that the pattern of intracellular accumulation of C-Dots was well in agreement with that of intracellular R6G accumulation.

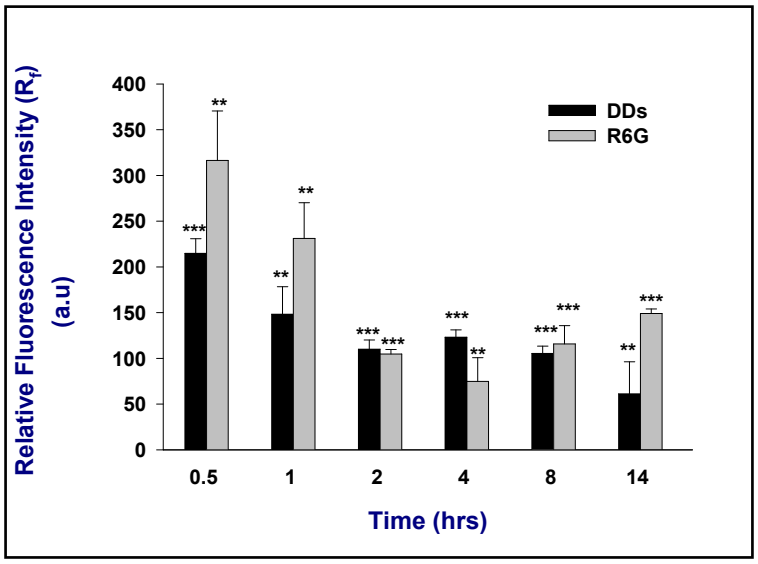

Fig. 5. Time-dependent cellular uptake of C-Dots by *Candida* cells measured by fluorescence intensity. The fungal cells were incubated with 4 mg/ml C-Dots and from this cell suspension, 10^7 cells were taken out at the following time points viz. 30 mins, 1 hr, 2 hrs, 4 hrs, 8 hrs and 14 hrs and cellular uptake of C-Dots by *Candida* cells were measured. R6G was used as positive control. The uptake of 10 µM R6G was monitored in the fungal cells after incubation for the corresponding time periods of 30 mins, 1 hr, 2 hrs, 4 hrs, 8 hrs and 14 hrs. Y axis depicts the mean relative fluorescence (Rf) values ± the standard deviation (SD) of three independent experimental sets. Relative Fluorescence (Rf) was calculated as before and the fluorescence intensity for cells incubated without C-Dots (blank) was subtracted from fluorescence intensity for cells incubated with C-Dots. *** represents $p<0.0001$ and ** represents $p<0.001$ calculated with respect to "no C-Dots" (control).

A bright blue fluorescence due to the internalization of the C-Dots into the fungal cells was clearly visible in the microscopy images after incubation with C-Dots (4 and 8 mg/ml)

respectively for 30 mins, 1 hr and 2 hrs (Fig. 6). It indicated that C-Dots could permeate throughout the fungal cells without imposing toxicity. Maximum cellular uptake of C-Dots was observed after 30 mins incubation time. No difference was observed in the intracellular uptake of C-Dots after incubation with C-Dots at concentrations of 4 mg/ml and 8 mg/ml (Fig. 6). R6G was used a positive control for assessing intracellular uptake. Green fluorescence inside the fungal cells indicated cellular uptake of R6G at different incubation time of 30 mins, 1 hr and 2 hrs (Fig. 6, panel D). The cells did not show any auto-fluorescence as revealed from Fig. 6 (panel A), indicating no hindrance from undesirable auto-fluorescence. The undesirable auto-fluorescence of cells certainly interferes and significantly affects conventional fluorophores whereas this study revealed that once incorporated into the cells, the self-fluorescence of the C-Dots remained distinctly different from the background of the cells and the medium, which is desirable for imaging applications. Thus, it can be unequivocally affirmed that the C-Dots synthesized in this study have potential for bioanalytical and biomedical applications. The C-Dots can be made more appropriate for targeted cellular imaging and live imaging applications by conjugation to different molecules/ drugs without altering the functions of C-Dots.

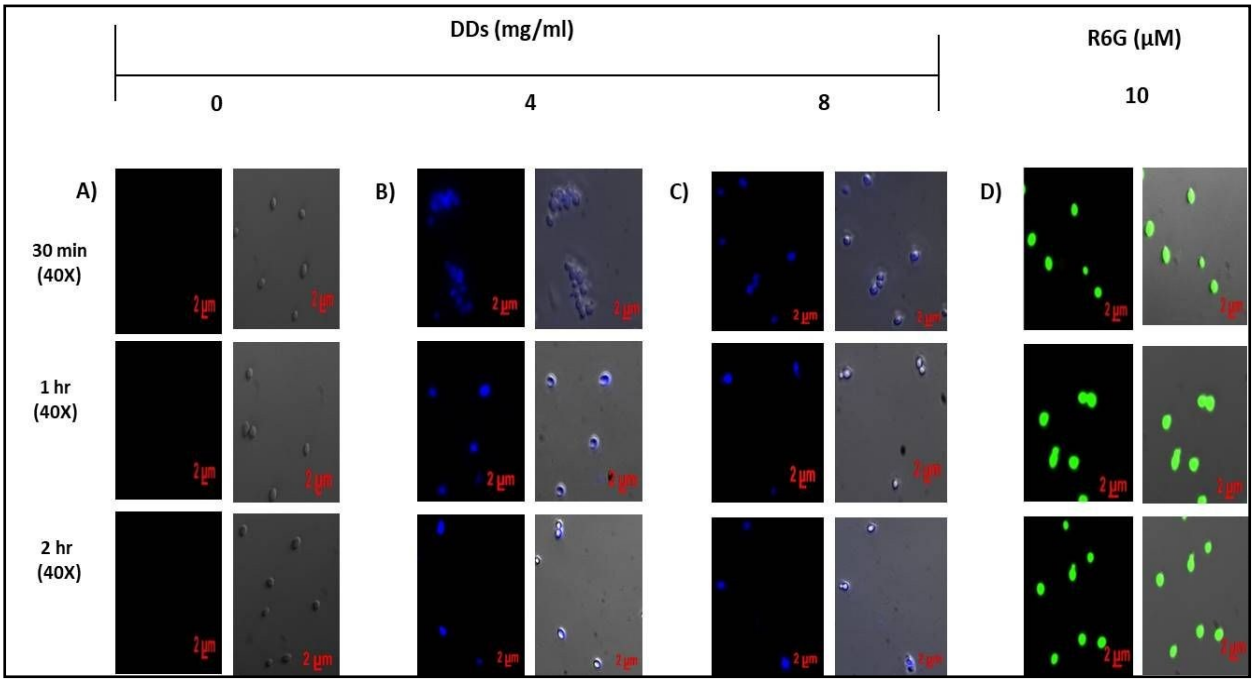

Fig. 6. Cellular uptake of C-Dots by fungal cells shown by Fluorescence microscopy. The images were taken after incubation of the fungal cells with 4 mg/ml and 8 mg/ml C-Dots for the time points viz. 30 mins, 1 hr and 2 hrs. The internalized C-Dots are indicated by the blue fluorescence visible within the fungal cells. R6G was used as positive control and the uptake of 10 μM R6G was observed as green fluorescence in the fungal cells after incubation for the same time periods of 30 mins, 1 hr and 2 hrs.

View Article Online
DOI: 10.1039/C9TB01863H

Viscoelastic Properties of DNA-C-Dot hydrogel

The viscoelastic profile of gel samples was evaluated from rheology using the following two different modes of analysis: (a) Isothermal frequency sweep studies were conducted to evaluate the shear induced deformation of gel structure (Fig. 7(a)), and (b) Isochronal temperature sweep studies were performed to determine melting profile of these gels. Frequency dependent behavior of gel samples is normally explained by linear viscoelastic theory and storage modulus G'which often displays a frequency ω dependent dispersion behavior given by[40]

$$G(\omega) = G_0\,\omega^{n'}; \qquad G_0 = \lim_{\omega \to 0} G(\omega) \qquad (2)$$

Here G_0 is low frequency elastic modulus. The fitting parameter n' varies between 0 and 2 for a viscoelastic material. It is 0 for a Hookean solid and 2 for a Maxwellian viscoelastic material.

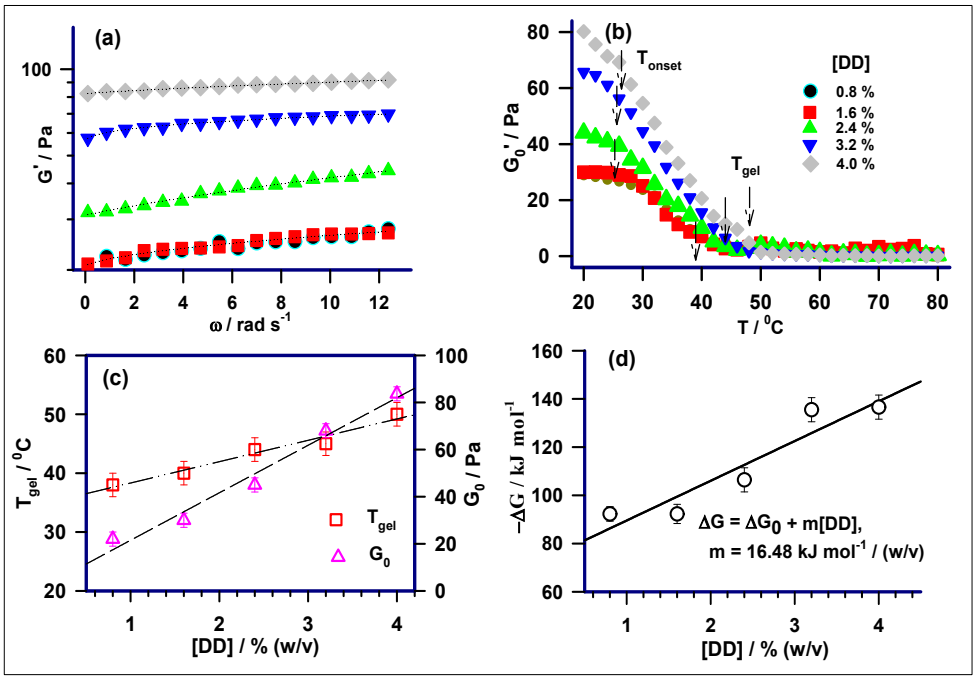

Fig. 7. Viscoelastic Properties of DNA- C-Dot (DDs) nanocomposite hydrogel: (a) Storage modulus as a function of frequency, (b) Temperature sweep profile, (c) Variation of T_{gel} and storage modulus, (d) Change in Gibbs free energy of gelation with C-Dot concentration.

It can be concluded from the data that G_0 had a value of ~ 20 Pa for a gel with 0.8 % C-Dot, and ~ 80 Pa for 4 % sample, the corresponding value of n' was 0.7 ± 0.2 (Fig. 7(c) and Fig. S5). For comparison, the reported G_0 value for DNA hydrogel is 20 ± 2 Pa and for ionogel,

it is 29 ± 2 Pa.[20,41] Thus, it can be stated that these C-Dot based DNA hydrogels were highly viscoelastic in nature with attributes dependent on the C-Dot content of the sample. It is to be noted that without the C-Dots, the samples would never gel. Therefore, these dots acted as crosslinkers in the DNA sol to generate a strong nanocomposite gel with tunable strength and melting temperature. The synergy of this interaction can be gauzed from the fact that the gel strength increased with C-Dot content.

In the next step, the melting profiles of the gels containing different concentration of C-Dots were evaluated and are depicted in Fig. 7(b). Dependence of T_{gel} and G_0 with C-Dot content is clearly shown in Fig. 7(c), which shows that both T_{gel} and G_0 increase highlighting the crosslinking efficiency of these dots, while retaining the viscoelastic nature of the gels.

The dot concentration [DD] could be correlated to the T_{gel} and G_0 through the linear relations given by

$$T_{gel}(DD) = T_{gel}(0) + m_{gel}(DD) \quad (3)$$

$$G_0(DD) = G_0(0) + m_{G0}(DD) \quad (4)$$

Where [DD] = 0 concentration values are represented as $T_{gel}(0)$ and $G_0(0)$, and the concentration coefficients are m_{gel} and m_{Go}, respectively. From the least-squares fitting of the data, we obtained: $T_{gel}(0) = 34.7\,^0C$, $G_0(0) = 1.33$ Pa, $m_{gel} = 3.6$ and $m_{Go} = 20.2$ with chi-squared value ~ 0.98.

The elastic energy stored in a network per unit volume is determined by its G_0 value. When this energy is equated with thermal energy, it defines a characteristic length scale called viscoelastic length. The length is a key parameter corresponding to self-assembled network, which is given by ζ_{el}[42]

$$G_0 \sim (k_B T)/\zeta_{el}^3 \quad (5)$$

This length varied (Fig. S5, Supplementary Information) from ζ_{el} = 58 nm for 0.8 % (w/v) of C-Dot containing DNA hydrogel sample to 37 nm for 4 % (w/v) C-Dot hydrogel. Therefore, the formed networks were denser at higher C-Dot concentration. The temperature sweep measurement (Fig. 7(b)) showed transition which can be referred as gelling temperature, T_{gel}. The T_{gel} value increased from 40 to 50°C with C-Dot concentration indicating sufficient interactions between DNA strands and C-Dot (Fig. 7(c)). Therefore, the gelling temperature of the nanocomposite gels can be tuned by altering the C-Dot concentration according to application. During the melting process, the equilibrium gel makes a thermodynamic transition to an equilibrium sol state. Therefore, the melting profile between T_{onset} and T_{gel} region (Fig. 7(b)) can be described by Arrhenius relation given by

View Article Online
DOI: 10.1039/C9TB01863H

$$\Delta G_0(T) = \Delta G_0 \, exp - \left(\frac{\Delta G}{RT}\right) \quad (6)$$

where, $\Delta G_0 = G_0(T_{onset}) - G_0(T_{gel})$, R is universal gas constant, T is temperature in Kelvin, $T_{onset} < T < T_{gel}$ is the melting region which was fitted to equation (6). The estimated Gibbs free energy of gelation ΔG varied from -90 to 140 kJmol^{-1} with increase in dot concentration, which clearly indicated more favourable networking in DNA gels (Fig. 7(d)). This reiterates our contention that these dots acted as crosslink junctions inside the gel matrix. The corresponding enthalpy (ΔH) and entropy (ΔS) change were estimated from the known values of free-energy and

$$\Delta G = \Delta H - T\Delta S \quad (7)$$

This analysis yielded, ΔH= -119 kJ mol^{-1} and ΔS= -5.16 J K^{-1} (Fig. S6, Supplementary Information). Thus, it was remarkable to note that DNA solution (1% (w/v)) transformed into a DNA hydrogel assisted by crosslinking junctions provided by DNA dots.

Morphology of DNA-C-Dot hydrogel

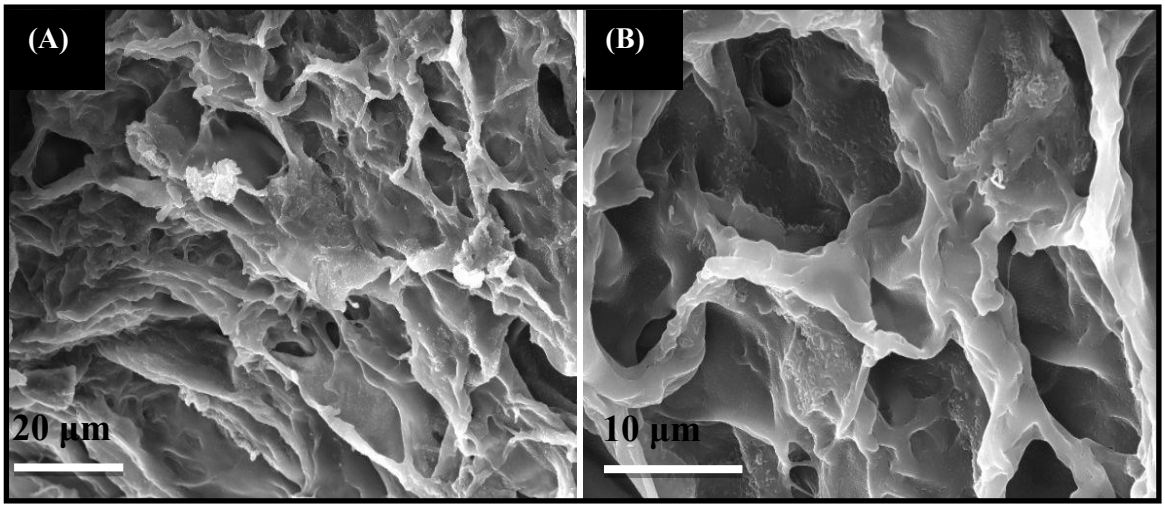

Fig. 8. Morphology of DNA- C-Dot hydrogel: (A) FESEM image with 20 µm and (B) 10 µm scale bar resolution.

The morphology of hydrogel as obtained from FESEM images is shown in Fig. 8. Interconnected networks and hierarchical porous structures were observed for these hydrogels, which again suggested that the DNA dots assisted in the evolution of self-assembled network structures from a solution that would otherwise not form a gel. A qualitative profile of the networks seen in these images can be realized from the estimation of network density in the gel concerned.

View Article Online
DOI: 10.1039/C9TB01863H

For a very good estimation in a given material, a good estimate of the network density υ can be derived from the G_0 data already known. In the Flory model, the network density is calculated from the equilibrium swelling experiments and can be determined approximately from the relation given by

$$E \approx \left({}^{3\rho RT}/_{2M_e}\right) \qquad (8)$$

where E is the low deformation Young's modulus,ρ is rubber density and M_e is the mean molecular weight of the polymer segment between crosslinks. Further, $\rho = \nu M_e$ and for an affine network, $E \approx 3G_0$ allows the above equation to be written as

$$\upsilon \approx \left({}^{2G_0}/_{RT}\right) \qquad (9)$$

The relative network density ν_r is given as

$$\nu_r = \left(\frac{\upsilon}{\upsilon_0}\right) \qquad (10)$$

where ν and ν_0 refer to the network density of the composite gel and DNA gel, respectively. The variation of ν_r with dot content is shown in Fig. S7 (Supplementary Information), which increases linearly with the dot concentration. This clearly establishes that the C-Dots played the role of crosslinkers in the gel network. It is pertinent to highlight the special features of the DNA-C-Dot gel *vis a vis* those of DNA hydrogel and DNA ionogel. Table 1 provides a comparison of physical properties of various DNA gels and their subtle distinctions.

Table 1. Comparison of DNA hydrogel, DNA-ionogel and DNA-C-Dot hydrogel. Parameters compared are gelation concentration C_{gel}, gelation temperature T_{gel}, storage modulus G_0, fluorescent nature, change in gelation free energy ΔG, viscoelastic length ξ_{el} and relative network density υ_r.

Parameters	Hydrogel[41]	Ionogel[20]	DNA-C-Dot gel	Speciality of DNA-C-Dot gel
C_{gel} / % (w/v)	2 %	1 %	1 %	lower gelation conc
T_{gel} / ^{0}C	34	60-65	40-50	Large gelation window
G_0 / Pa	20	27-70	20-80	Large gel strength window
ξ_{el} /nm	59	38-45	36-58	Tunable porous gel
ΔG/kJ	-35	-33 to -78	-90 to -140	Strongly free-energy driven

υ_r	1	1.35-3.5	1-4.2	Heavily crosslinked
Fluorescence	None	None	Yes	Fluorescent gel

Dopamine detection

For the electrochemical study, the sol was drop cast on the ITO plate to form a thin film at room temperature. The electrochemical response of DNA-C-Dot hydrogel/ ITO electrode was observed in 0.05 to 0.5 V potential ranges. The CV profile of bare ITO and DNA-C-Dot hydrogel/ ITO electrode at 50 mV/s scan rate was investigated to understand the electrochemical behavior in Zobell's solution. It was observed that the peak current of hydrogel/ ITO electrode was higher in comparison to the ITO. This suggested the presence of thin film on the ITO surface and a reduction in electron transfer accessibility by the film compared to ITO electrode (Fig. 9(a)).[43,44] The sole objective of this measurement was to analyze the potential ability of the electrodes towards selective detection of bioanalyte Dopamine in the presence of interferents like, Urea (U), Citric acid (CA), L-cysteine (L-cys), and Glycine (Gly). The study of the electrochemical response of these electrodes for bioanalytes was undertaken within the concentration range of 0.2-2.0 mM and at a fixed scan rate of 50 mV/s. The observed change in anodic and cathodic peak current with variations in analyte concentration helped to determine response of the electrode towards bioanalyte tested. A single DNA-C-Dot hydrogel/ ITO electrode was used for detection of whole range of concentration of a given analyte. Distinct changes in CV profiles were observed in the case of Dopamine while no major changes were seen in the case of other tested analytes. The anodic peak current was found to increase with increasing concentration of Dopamine. Additionally, a shift of anodic peak or current towards higher potential was observed with increasing Dopamine concentration (see Fig. 9 (b)). It thus, clearly indicated an increase in the oxidation (Ia) and reduction (Ic) current on treatment with Dopamine, which suggested that the electro-catalytic reaction was because of the presence of Dopamine (Fig. 9 (c)). No change in the peak current was found for other bioanalytes even at very high concentration of 2.0 mM (data not shown). The linear regression equation for wide range of analyte is, I (μA) = 186 + 149XC (mM) with R^2= 0.96. Sensitivity for the electrode obtained was 0.6 μA μM^{-1} cm^{-2} and the detection limit was $5X10^{-3}$ mM.

View Article Online
DOI: 10.1039/C9TB01863H

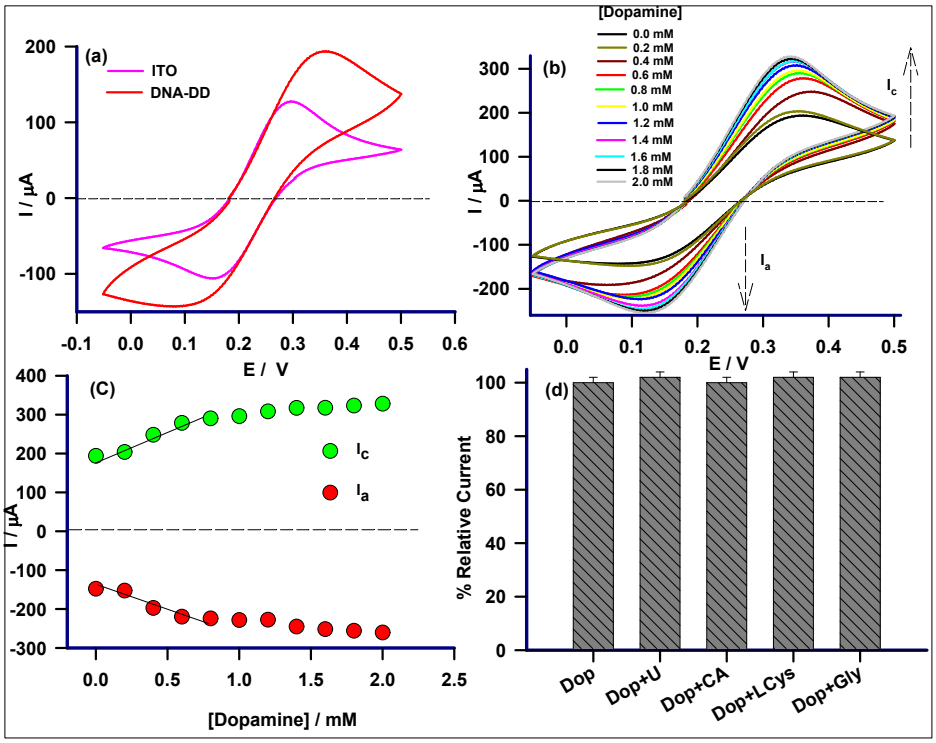

Fig. 9. Response of C-Dot (DD) based electrochemical sensor. (a) Electrochemical response of Blank ITO electrode and DND-C-Dot hydrogel/ ITO electrode without analyte, (b) Electrochemical response of hydrogel/ ITO electrode towards Dopamine for -0.05 to 0.5 Voltage range, (c) Anodic and cathodic peak current for different Dopamine concentrations. Fitting line shown corresponds to the linear fitting of dopamine detection range, and (d) Interference histogram shows selective response for Dopamine.

The selectivity of the electrode (Fig.9(d)) was monitored by potential interferents. The study was performed at a scan rate 50 mV s^{-1} taking 1:1 Dopamine and the normal physiological concentration of interferents viz. Urea, Citric acid, L-cysteine, and Glycine. We found that this electrochemical sensor electrode was specific to Dopamine detection and did not respond to presence of other analytes. In order to place our results in the proper perspective, a list is provided in Table 2 where figures of merit of various reported methods are compared. Our method offers a wider linear range of detection with low detection limit, in addition to the detection platform being green.

Table 2. Comparison of different electrodes used for Dopamine detection.

View Article Online
DOI: 10.1039/C9TB01863H

Sample	Linear range /mM	Detection limit /mM	Reference
AgNPs/rGO	0.01-0.8	$5.4X10^{-3}$	45
Gold Nanoelectrode	0.001-0.1	$5.8\ X10^{-3}$	46
PANI-NF/Pt	0.062-0.6.	$33.3X10^{-3}$	47
RGO/TiO_2	0.002–0.06	$6X10^{-3}$	48
DNA-DD/ITO	0-1.0	$5X10^{-3}$	Present work

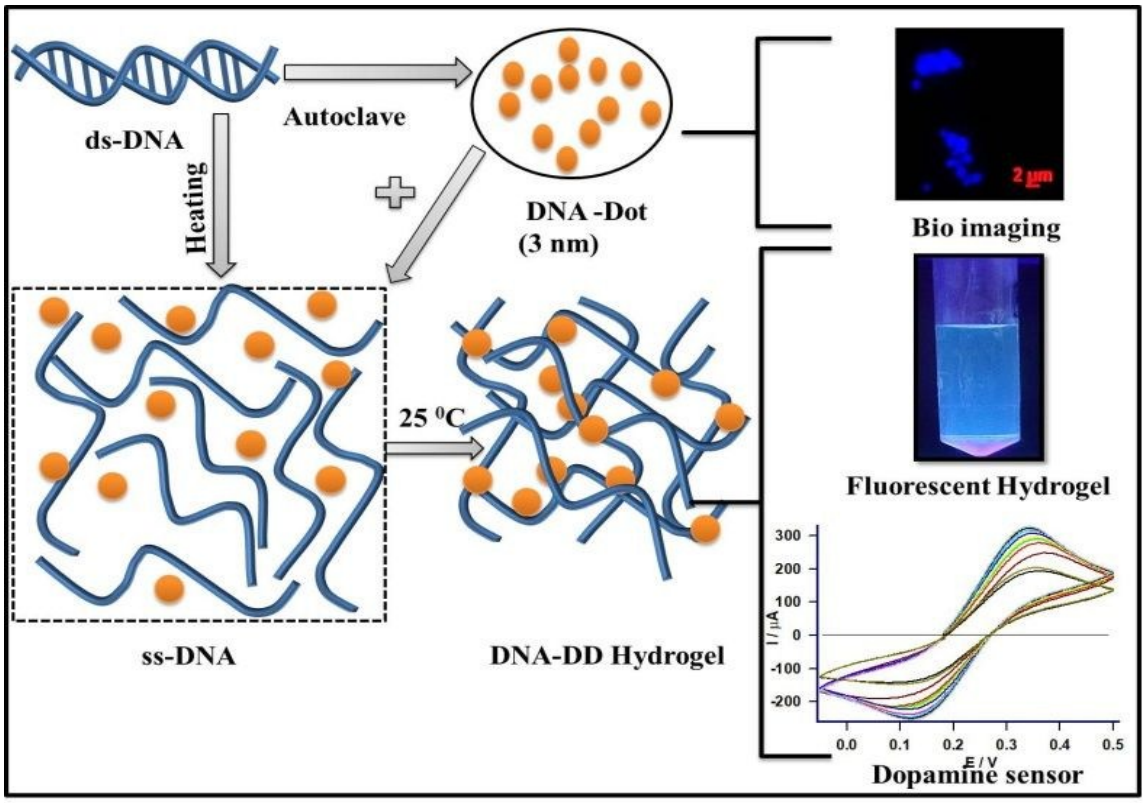

Scheme 1: Illustration for multifunctionality of C-Dots (DD): bioimaging, fluorescent DNA hydrogel and dopamine sensing.

Conclusion

To summarize, combining the unique properties of DNA, we developed water soluble, biocompatible carbon dots of size 4-5 nm for multifunctional applications (see Graphical abstract). This study describes facile and green synthesis of hydrophilic, blue fluorescence

View Article Online
DOI: 10.1039/C9TB01863H

emitting carbon dots by hydrothermal route from Salmon testes DNA. As expected these C-Dots exhibited excitation dependent emission (Fig.2) with mean quantum yield of about 40% (See Supplementary Information for details). Unlike previous studies on use of DNA based carbon dots for bioimaging and drug delivery vehicles, we have demonstrated multipurpose applications of these dots viz. bioimaging, dots based hydrogel for drug delivery and biosensing applications (a comparison is provided in Table III). The application of C-Dots in bioimaging was demonstrated using microbial pathogen, *Candida albicans*. These C-Dots exhibited negligible cytotoxicity and efficiently internalized into microbial cells. The C-Dots possess good PL stability and high biocompatibility and can be used as nontoxic fluorescent probe for bioimaging. There is a lack of fluorescent trackers for study of drug-pathogen interactions and microbial drug resistance. C-Dots possess potential for further exploitation in microbial studies after conjugation with desired molecules and drugs. This would make C-Dots more appropriate for targeted cellular imaging and live imaging applications, such as for study of drug kinetics (uptake and efflux) and localization during multi drug resistance in microbes, for efficient drug delivery and wound healing purposes.

In addition, we also synthesized DNA-C-Dot low concentration fluorescent hydrogel with same DNA which is unique in this work and such hydrogels are more versatile for drug delivery and therapy applications with potential to replace previously reported toxic QD based hydrogels.[7] C-Dots acted as pseudo crosslinker for the same DNA to form nanocomposite hydrogel at low DNA concentration (1 % w/v). The strength of these gels varied from 20-80 Pa and melting temperature from 40 ^{0}C to 50 ^{0}C, tunable with dot content. The viscoelastic length of these hydrogel decreased from 58 to 36 nm which corresponds to a denser network formation with increase in dot concentration. These hydrogels showed blue fluorescence under UV light. Apart from this, we required less number of chemicals, rather only DNA for preparing such hydrogel.

This study also demonstrated use of carbon dots made from based DNA hydrogels for electrochemical sensing. The these electrodes displayed selective detection of dopamine, which can be developed into a good sensing platform. Thus, it can be concluded that multimodality of such C-Dot based nanostructures has potential to serve as smart systems for bioimaging, low concentration non-toxic fluorescent DNA hydrogel and biosensing.

Table 3. Comparison of DNA dots reported in other studies.

View Article Online
DOI: 10.1039/C9TB01863H

Sample	Application	Reference
DNA biodot	• Used for imaging of HER2 over-expressing human breast cancer cell line MCF7 (MCF7/HER2) and checked biocompatibility	15
DNA-carbon dot (Prepared using genomic DNA isolated from *E. coli*as source material)	• Used for imaging of epithelial cell line from human kidney embryo (HEK 293) • Internalization checked in non-pathogenic microbes, *E. coli* and *Saccharomyces cerevisiae* for future cell related studies • Evaluated the DNA-carbon dots as fluorescent delivery vehicles by using Rhodamine 6G and Doxorubicin for *S. cerevisiae* and using Propidium iodide for *S. cerevisiae* and HEK 293 cells.	16
DNA Dots (Prepared using Salmon testes DNA (2000 bp, ds DNA) as source material)	Evaluated cellular internalization and microbial toxicity using the fungal opportunistic pathogen, *Candida albicans*; which possess potential for further exploitation in microbial studies after conjugation with desired molecules and drugs, thus making them more appropriate for targeted cellular imaging and live imaging applications, such as for study of drug kinetics (uptake and efflux) and localization during multi drug resistance in microbes, for efficient drug delivery and wound healing purposes. • Assessed reactive oxygen species generation which was as low as control cells, thus appearing to be a major contributory factor for the non-toxic, biocompatible nature. • Low concentration hydrogel was prepared with same DNA, which can replace toxic quantum dot based hydrogel for drug delivery, bioimaging and sensing applications • Demonstrated use of DNA dots based hydrogel for electrochemical sensing. e.g Dopamine sensing	This study

Funding Information: PP acknowledges UGC-BSR, India for Senior Research Fellowship and Preeti acknowledges CSIR, India for Junior Research Fellowship. KR is thankful to Department of Science and Technology, Government of India-Inspire Faculty

View Article Online
DOI: 10.1039/C9TB01863H

Award. This research was supported by Department of Science and technology, India (DST-PURSE-II and EMR/2016/004868) for funding. TP acknowledges Indian Funding Agencies- University Grants Commission (UGC) JNU-UPoEII and Department of Science and Technology (DST) (JNU-DST-PURSE-II).

Conflicts of interest

Authors declare no conflict of interest.

References

1 Y. Zhang, J. Tu, D. Wang, H. Zhu, S. K. Maity, X. Qu, B. Bogaert, H. Pei and H. Zhang, *Adv. Mater.*, 2018, **30**, 1–44.

2 J. Kondo, Y. Tada, T. Dairaku, Y. Hattori, H. Saneyoshi, A. Ono and Y. Tanaka, *Nat. Chem.*, 2017, **9**, 956–960.

3 R. Schreiber, J. Do, E. Roller, T. Zhang, V. J. Schu¨ller, P. C. Nickels, J. Feldmann and T. Liedl, *Nat. Nanotech.*, 2014, **9**, 74–78.

4 U. Resch-Genger, M. Grabolle and S. e. al. Cavaliere-Jaricot, *Nat. Methods*, 2008, **5**, 763–775.

5 C. Tzu-Heng and T. Wei-Lung, *Anal. Chem.*, 2017, **89**, 11348–11356.

6 X. Sun and Y. Lei, *Trends in Anal. Chem.*, 2017, **89**, 163–180.

7 L. . Zhang, S. R. . Jean, S. . Ahmed, P. M. . Aldridge, X. . Li, F. . Fan, E. H. . Sargent and S. O. Kelley, *Nat. Comm.*, 2017, **8**, 381.

8 O. E. Semonin, J. M. Luther, S. Choi, H. Chen, J. Gao, A. J. Nozik and M. C. Beard, *Science (80-.).*, 2011, **334**, 1530–1533.

9 J. P. Clifford, G. Konstantatos, K. W. Johnston, S. Hoogland, L. Levina and E. H. Sargent, *Nat. Nanotech.*, 2009, **4**, 40–44.

10 Y. Ma, M. Wang, W. Li, Z. Zhang, X. Zhang, T. Tan, X. Zhang and Z. Cui, *Nat. Comm.*, 2017, **8**, 1–8.

11 J. Wang, G. Liu, K. C. Leung, R. Loffroy, P. Lu and Y. X. J. Wáng, *Curr Pharm Des*, 2015, **21**, 5401–5416.

12 S. Fasbender, S. Allani, C. Wimmenauer, R.-P. Cadeddu, R. K., J. C. Fischer, B. Bulat, M. Luysberg, C. A. M. Seidel, T. Heinzel and R. Haas, *RSC Adv.*, 2017, **7**, 12208–12216.

13 T. S. Atabaev, Nanomaterials, 2018, 8, 342; doi:10.3390/nano8050342

View Article Online
DOI: 10.1039/C9TB01863H

14 B. De and N. Karak, RSC Adv., 2013, 3, 8286-8290

15 C. X. Guo, J. Xie, W. Wang, X. Zheng, H. B. Yang and C. Ming L, *Sci. Rep.*, 2013, **3**, 1–6.

16 H. Ding, F. Du, P. Liu, Z. Chen and J. Shen, *ACS Appl. Mater. Interfaces*, 2015, **7**, 6889–6897.

17 S. H. Um, J. B. Lee, N. Park, S. Y. Kwon, C. C. Umbach and D. Luo, *Nat. Mater.*, 2006, **5**, 797–801.

18 J. B. Lee, S. Peng, D. Yang, Y. H. Roh, H. Funabashi, N. Park, E. J. Rice, L. Chen, R. Long, M. Wu and D. Luo, *Nat. Nanotechnol.*, 2012, **7**, 816–820.

19 H. Qi, M. Ghodousi, Y. Du, C. Grun, H. Bae, P. Yin and A. Khademhosseini, *Nat. Comm.*, 2013, **4**, 1–10.

20 P. K. Pandey, K. Rawat, V. K. Aswal, J. Kohlbrecher and H. B. Bohidar, *Phys. Chem. Chem. Phys.*, 2017, **19**, 804–812.

21 S. Liu, F. Shi, X. Zhao, L. Chen and X. Su, *Biosens. Bioelectron.*, 2013, **47**, 379–384.

22 D. Lakshmi, A. Bossi, M. J. Whitcombe, I. Chianella, S. A. Fowler, S. Subrahmanyam, E. V. Piletska and S. A. Piletsky, *Anal. Chem.*, 2009, **81**, 3576–3584.

23 H. Tanga, P. Lina, H. L. W. Chana and F. Yana, *Biosens. Bioelectron.*, 2011, **26**, 4559– 4563.

24 I. Gualandi, D. Tonelli, F. Mariani, E. Scavetta, M. Marzocchi and B. Fraboni, *Sci. Rep.*, 2016, 1–10.

25 K. Rawat, V. K. Aswal and H. B. Bohidar, *J. Phys. Chem. B*, 2012, **116**, 14805–14816.

26 B. J. Berne and R. Pecore, *Dynamic light scattering with applications to Chemistry, Biology and Physics*, John Wiley & Sons, INC, New York, 1976.

27 W. A. Fonzi and M. Y. Irwin, *Genetics*, 1993, **134**, 717–728.

28 J. H. Rex, B. D. Alexander and D. et al. Andes, *Reference Method for Broth Dilution Antifungal Susceptibility Testing of Yeasts*, Clinical and Laboratory Standards Institute (CLSI), 950 West Valley Road, Suite 2500, Wayne, Pennsylvania, USA., 3rd edn., 2008.

29 T. Prasad, A. Chandra, C. K. Mukhopadhyay and R. Prasad, *Antimicrob Agents Chemother*, 2006, **50**, 3597–3606.

30 T. Prasad, S. Hameed and R. et al. Manoharlal, *FEMS Yeast Res.*, 2010, **10**, 587–596.

31 S. Sanwalani, K. Rawat, M. Pal, H. B. Bohidar and A. K. Verma, *J. Nanopart Res.*, 2014, **16**, 2382–2386.

View Article Online
DOI: 10.1039/C9TB01863H

32 A. L. Patterson, *Phys. Rev.*, 1939, **36**, 978–981.
33 J. . Tauc, R. . Grigorovici and A. Vancu, *Phys. Stat. sol.*, 1966, **15**, 627–637.
34 H. Ding, J. S. Wei, N. Zhong, Q. Y. Gao and H. M. Xiong, *Langmuir*, 2017, **33**, 12635–12642.
35 Z. L. Wu, Z. X. Liu and Y. H. Yuan, *J. Mater. Chem. B*, 2017, **5**, 3794–3809.
36 V. D. Matteis, M. Cascione, C. C. Toma and S. Leporatti, *Nanomaterials*, 2018, **8**, 1–23.
37 C. Fu, K. Qian and A. Fu, *Mater. Sci. Eng. C Mater Biol. Appl.*, 2017, **76**, 350–355.
38 N. Zhou, S. Zhu, S. Maharjan, Z. Hao, Y. Song, X. Zhao, Y. Jiang, B. Yang and L. Lu, *RSC Adv.*, 2014, **4**, 62086−62095.
39 S. Forster, A. E. Thumser, S. R. Hood and N. Plant, *PLoS One*, 2012, **7**, 1–9.
40 H. A. Barnes, *A Handbook of Elementry Rheology*, University of Wales, Institute of Non-Newtonian fluid Mechanics, Aberystwyth, 2000.
41 N. Arfin, V. K. Aswal, J. Kohlbrecher and H. B. Bohidar, *Polymer*, 2015, **65**, 175–182.
42 A. Ajji and L. Choplin, *Macromolecules*, 1991, **24**, 5221–5223.
43 N. Joshi, K. Rawat, P. R. Solanki and H. B. Bohidar, *Sens. BIO-SENSING Res.*, 2015, **5**, 105–111.
44 N. Joshi, K. Rawat, P. R. Solanki and H. B. Bohidar, *Biochem. Eng. J.*, 2015, **102**, 69–73.
45 B. Kaur, T. Pandiyan, B. Satpati and R. Srivastava, *Colloids Surfaces B Biointerfaces*, 2013, **111**, 97– 106.
46 D. Kim, E. Kang, S. Baek, S. Choo, Y. Chung, D. Lee, J. Min and T. Kim, *Sci. Rep.*, 2018, **8**, 14049.
47 H. N. Yu, Y. C. Pang and J. Y. Tang, *Int. J. Electrochem. Sci.*, 2015, **10**, 8353 – 8360.
48 T Peik-See, A Pandikumar, H Nay-Ming, L Hong-Ngee, Y Sulaiman Sensors, 2014, **14**, 15227-15243